Available online at www.sciencedirect.com
ScienceDirect
Journal of Geodynamics 42 (2006) 194–209
JOURNAL OF GEODYNAMICS
http://www.elsevier.com/locate/jog

Analysis of central western Europe deformation using GPS and seismic data

Magdala Tesauro *, Christine Hollenstein, Ramon Egli, Alain Geiger, Hans-Gert Kahle

Geodesy and Geodynamics Laboratory, ETH Zürich, Switzerland

Received 1 November 2005; received in revised form 28 June 2006; accepted 11 August 2006

Abstract

The kinematic field of central western Europe is characterized by relatively small movements (around 1–2 mm/year) and diffuse seismicity with earthquakes occurring mostly in the shallow crust (within 15 km), prevalently concentrated along the Alps and the European Cenozoic Rift System (ECRIS). In order to study and constrain the current crustal kinematic field we reconstructed the velocity and the strain field using permanent GPS stations, belonging to different networks (AGNES, EUREF, REGAL, RGP). The 2D strain rate tensor has been calculated using the method of least-squares collocation. Our results show that the area of maximum compression is located along the Alpine chain, where maximum values of 7 ± 2 nstrain/year are found, while maximum extension is measured between the Armorican Massif and the Massif Central, where values of 4 ± 2 nstrain/year are reached.

The earthquakes with $M > 3.0$, have been used to estimate the seismic strain rates, while the style of the seismic deformation was reconstructed from the fault plane solutions (FPS) available from the literature. Relatively high values of seismic strain rates (around 10 nstrain/year) are measured along the Alpine Chain and the ECRIS. Results obtained by geodetic and seismic data are quite in agreement and reflect the different tectonic evolution of the geological features characterizing the area of study. The orientation of the compressional geodetic and seismic strain axes are NW-SE in most of the area of study, on account of the action of plate boundary forces. A rotation of the same axes to N-S direction along the eastern Alps, possibly related to the Adria convergence, is found.

Keywords: Tectonics; GPS; Seismic; Strain field; Geophysics

1. Introduction

This work, carried out in the framework of the European Union funded ENvironmental TECtonics (ENTEC) research and training network, and the EUCOR-URGENT (Upper Rhine Graben Evolution Neo Tectonics) project, was concerned with the kinematic interpretation of central western Europe area and in particular of the Rhine Graben area, using the results of GPS and seismic data. Following this purpose, first we reconstruct the velocity and the strain rates of the area of study using GPS data, collected at permanent stations, spanning from 1996 to 2004 (Table 1)

* Corresponding author. Present address: Faculty of Earth & Life Sciences, Vrije Universiteit De Boelelaan 1085, 1081 HV Amsterdam, The Netherlands. Tel.: +31 205987374; fax: +31 205989943.
E-mail address: magdala.tesauro@falw.vu.nl (M. Tesauro).

0264-3707/$ – see front matter © 2006 Elsevier Ltd. All rights reserved.
doi:10.1016/j.jog.2006.08.001

and we compare these results with the ones previously obtained by ourselves and other authors. Moreover, we use the focal mechanisms, obtained by different authors, to reconstruct the variation of the tectonic regime, while the seismic parameters of the earthquakes with $M > 3.0$, are used to estimate the seismic strain rates. The distribution of the geodetic and seismic strain rates highlights the difference in the evolution of the geological features present the area of study.

2. Geological setting

Central western Europe includes geological units different for age, origin, evolution and recent activity. Moreover, it is tectonically more active than it could be expected from its location far away from any plate boundaries, being characterized by moderate seismicity and crustal velocity of the order of 1–2 mm/year (Nocquet et al., 2001; Nocquet and Calais, 2003; Tesauro et al., 2005). The activity is probable attributable to stress associated with the forces acting at the plate boundaries, which can cause earthquakes along pre-existing weakness, and effects of regional mantle processes underneath this area (Goes et al., 2000b).

One of the main structural units of this area are the Alps (Fig. 1). They represent the western European segment of the Tertiary collision zone between the African and the Eurasian continents (Fig. 1). N-S convergence between the African and the Eurasian plates began approximately 120 Myear ago and was related to a counterclockwise rotation of the African plate. After the Alpine Tethys ocean, which lay in between Eurasia and the Adriatic microplate, had been subducted to the south, the two continents collided in the area of the eastern Alps at about 65 My (Schmid et al., 1996, 1997). As convergence continued, the upper crustal parts of the Adriatic continental microplate were thrust over the oceanic and European crust while the lower Adriatic crust and upper mantle intruded into Eurasia, splitting the Eurasian crust horizontally (Pfiffner et al., 1997). During the early Miocene (about 23 My), the continuing indentation of the Adriatic plate caused the uplift of the Alps, while the debris of the rising mountains were deposited in the foreland basin to the north to form the Molasse Basin (Fig. 1). Continued compressional deformation formed the Jura

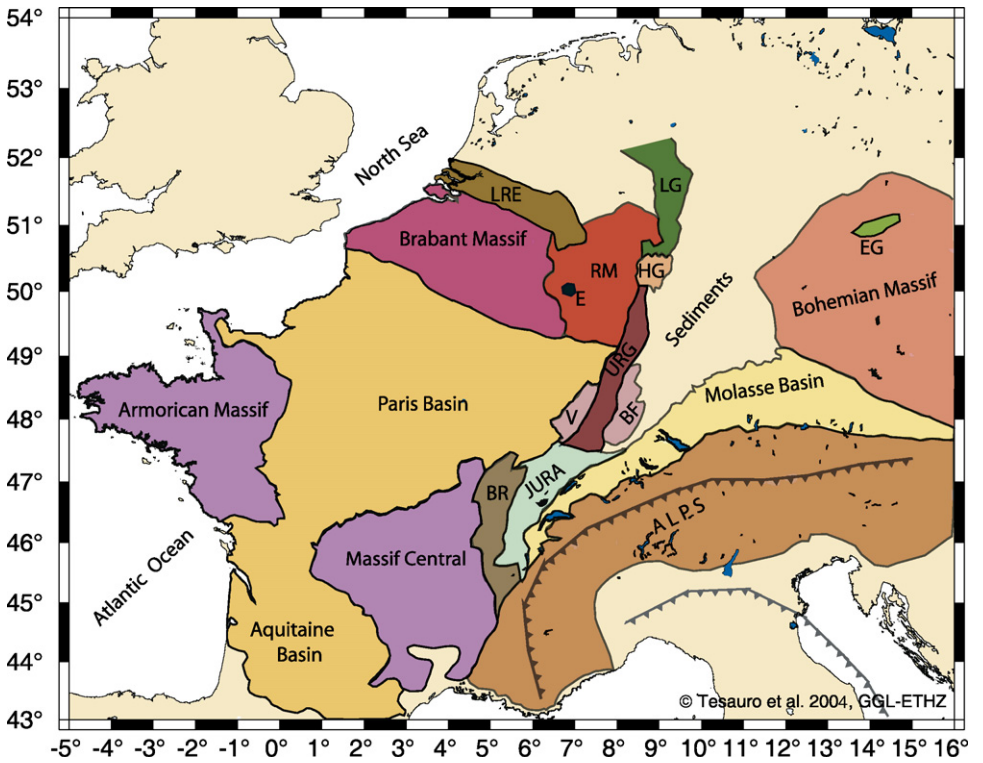

Fig. 1. Principal geological units of central western Europe. BR: Bresse-Rhône Depression, V: Vosges, BF: Black Forest, URG: Upper Rhine Graben, HG: Hessen Graben, LG: Leine Graben, RM: Rhenish Massif, E: Eifel, LRE: Lower Rhine Embayment, EG: Eger Graben (Tesauro et al., 2005).

Table 1
Residual values between the ITRF2000 velocities and the rotation of the Eurasian plate from the combination of the AGNES, EUREF, REGAL and RGP permanent GPS networks

Name	Initial time	Final time	n weeks	Latitude	Longitude	V_{north}	V_{east}	V_{abs}	σ_{north}, σ_{east}
ARDE	11/28/2001	05/19/2004	126	46.78	10.20	1.2	−0.8	1.4	0.6
BOUR	02/07/2001	05/19/2004	160	47.39	7.23	0.3	−0.5	0.6	0.6
BRST	04/17/2002	05/19/2004	91	48.38	−4.50	0.5	−0.2	0.6	0.8
BSCN	04/17/2002	05/19/2004	108	47.25	5.99	1.0	−0.4	1.1	0.7
DAVO	09/09/1998	05/19/2004	297	46.81	9.84	1.3	−0.5	1.4	0.4
DOUR	10/24/2001	05/19/2004	132	50.09	4.59	−0.6	−1.0	1.1	0.6
EGLT	04/17/2002	05/19/2004	110	45.40	2.05	−0.4	−0.4	0.6	0.7
EPFL	01/27/1999	10/22/2003	228	46.52	6.57	2.1	0.2	2.1	0.5
ETHZ	09/02/1998	05/19/2004	273	47.41	8.51	0.7	−0.2	0.8	0.4
EXWI	01/26/2000	05/19/2004	225	46.95	7.44	−0.7	−0.4	0.8	0.5
FALE	12/26/2001	05/19/2004	126	46.80	9.23	1.6	−0.4	1.7	0.6
FCLZ	03/22/2000	05/19/2004	202	45.64	5.99	0.8	−0.3	0.9	0.5
FHBB	09/02/1998	05/19/2004	291	47.53	7.64	0.7	0.0	0.7	0.4
FRIC	01/03/2001	05/19/2004	177	47.53	8.11	0.3	−0.4	0.5	0.5
GENE	12/13/2000	05/19/2004	180	46.25	6.13	0.8	−0.8	1.1	0.5
GRAS	04/30/2003	05/19/2004	55	43.75	6.92	1.2	−0.2	1.2	1.1
GRAZ	05/09/2001	05/19/2004	159	47.07	15.49	0.9	0.1	0.9	0.6
HFLK	09/02/1998	01/14/2004	233	47.31	11.39	1.5	−0.4	1.5	0.5
HOHT	12/13/2000	05/19/2004	180	46.32	7.76	0.9	−0.3	0.9	0.5
HUTT	02/14/2001	05/19/2004	153	47.14	7.83	0.6	−0.2	0.6	0.6
JUJO	09/02/1998	05/19/2004	299	46.55	7.98	−0.1	−0.6	0.6	0.4
KARL	05/09/2001	05/19/2004	159	49.01	8.41	0.7	0.2	0.7	0.6
KREU	12/19/2001	05/19/2004	127	47.64	9.16	0.5	−0.4	0.7	0.6
LILL	04/17/2002	05/19/2004	74	50.61	3.14	0.5	−1.2	1.3	0.8
LOMO	09/02/1998	05/19/2004	299	46.17	8.79	0.9	−0.6	1.1	0.4
LUZE	01/03/2001	05/19/2004	177	47.07	8.30	1.2	−0.3	1.2	0.5
MANS	04/17/2002	05/19/2004	110	48.02	0.16	0.4	−1.1	1.2	0.7
MARS	03/08/2000	05/19/2004	209	43.28	5.35	0.9	−0.7	1.1	0.5
MART	06/12/2002	05/19/2004	102	46.12	7.07	1.2	−1.0	1.6	0.7
MLVL	04/17/2002	05/19/2004	110	48.84	2.59	−0.1	−0.6	0.6	0.7
MODA	03/22/2000	05/19/2004	206	45.21	6.71	0.5	−0.7	0.8	0.5
NANT	04/17/2002	07/23/2003	37	47.15	−1.65	−0.7	−0.3	0.7	1.2
NEUC	09/27/2000	05/19/2004	190	46.99	6.94	0.5	−0.4	0.6	0.5
PADO	11/28/2001	05/19/2004	121	45.41	11.90	1.6	−0.8	1.8	0.7
PAYE	09/20/2000	05/19/2004	185	46.81	6.94	0.1	−0.1	0.2	0.5
PFAN	10/27/1999	03/17/2004	225	47.52	9.78	2.0	−1.2	2.3	0.5
RENN	04/17/2002	05/19/2004	109	48.11	−1.67	−0.1	−1.0	1.0	0.7
SAAN	11/28/2001	05/19/2004	130	46.52	7.30	0.2	0.2	0.2	0.6
SAME	11/28/2001	05/19/2004	110	46.53	9.88	0.7	−0.3	0.7	0.7
SANB	12/05/2001	05/19/2004	125	46.46	9.18	1.6	−1.2	2.0	0.6
SBGZ	03/08/2000	04/07/2004	149	47.80	13.11	1.2	−0.2	1.2	0.6
SCHA	01/03/2001	05/19/2004	177	47.74	8.66	0.4	0.1	0.4	0.5
SJDV	09/02/1998	05/19/2004	286	45.88	4.68	0.5	0.0	0.5	0.4
STAB	12/05/2001	05/19/2004	129	45.86	8.94	1.4	−1.8	2.2	0.6
STCX	09/19/2001	05/19/2004	140	46.82	6.50	0.9	−0.8	1.2	0.6
STGA	12/13/2000	05/19/2004	178	47.44	9.35	0.6	−0.5	0.8	0.5
STRA	03/22/2000	05/19/2004	193	48.62	7.68	0.3	−0.2	0.3	0.5
TORI	03/08/2000	05/19/2004	219	45.06	7.66	0.6	−0.2	0.6	0.5
UZNA	01/03/2001	05/19/2004	177	47.22	9.01	0.9	−0.1	0.9	0.5
VENE	01/31/2001	05/19/2004	171	45.44	12.33	1.9	0.0	1.9	0.6
VFCH	04/17/2002	05/19/2004	109	47.29	1.72	−0.7	0.2	0.7	0.7
WTZR	09/02/1998	05/19/2004	299	49.14	12.88	0.6	−0.3	0.6	0.4
ZIMM	09/02/1998	05/19/2004	299	46.88	7.47	0.9	−0.2	0.9	0.4
BRUS	08/05/1996	05/24/2004	405	50.80	4.36	0.2	−0.5	0.5	0.4
DELF	08/05/1996	05/24/2004	405	51.99	4.39	0.3	−0.5	0.6	0.4

Table 1 (*Continued*)

Name	Initial time	Final time	*n* weeks	Latitude	Longitude	V_{north}	V_{east}	V_{abs}	σ_{north}, σ_{east}
DRES	12/27/1999	05/24/2004	230	51.03	13.73	0.8	−0.7	1.0	0.5
EIJS	06/19/2000	05/24/2004	205	50.76	5.68	0.6	−0.7	0.9	0.5
GOPE	08/05/1996	05/24/2004	355	49.91	14.79	0.5	−0.5	0.8	0.4
KOSG	08/05/1996	05/24/2004	405	52.18	5.81	0.6	−0.3	0.7	0.4
OBE2	12/24/2001	05/24/2004	126	48.09	11.28	0.7	−0.6	0.9	0.6
POTS	05/19/1997	05/24/2004	366	52.38	13.07	0.1	−0.5	0.5	0.4
PTBB	05/08/2000	05/24/2004	207	52.30	10.46	1.0	0.3	1.1	0.5
WSRT	10/13/1997	05/24/2004	345	52.91	6.60	0.8	−0.5	0.9	0.4

The stations belonging to the Swisstopo and EUREF datasets are displayed in black and in grey, respectively. The following parameters are reported: initial and final time of observation displayed as month, day and year, the number of weeks in which a GPS result was existing, latitude and longitude expressed in decimal degree, V_{north}, V_{east}, V_{abs}, $\sigma_{V_{north}}$ and $\sigma_{V_{east}}$, the horizontal velocity components, the absolute value of velocity and the standard deviations of the horizontal velocity components, respectively, expressed in mm/year.

Mountains (Fig. 1) around 3–5 My and resulted in the most recent tectonic movements north of the Alps which affected the foreland basin. Whether the foreland is still active as a fold and thrust belt (Meyer et al., 1994; Calais, 1999) or whether this deformation has ceased or changed is subject to debate (Becker, 1999). Present convergence rates of up to 6 mm/year have been estimated for the relative motion between Africa and Europe (DeMets et al., 1994).

NW to the Alpine chain, the Upper Rhine Graben (URG) represents the central most prominent segment of the European Cenozoic rift system (ECRIS) of Eocene age (Fig. 1). The ECRIS extends from the North Sea to the Mediterranean coast through Germany and France over a distance of about 1100 km and it is likely formed in a region of pre-existing Hercynian zones of weakness (Achauer and Masson, 2002) (Fig. 1). This tensile episode can be related to Alpine tectonics and Africa–Eurasia collision (Achauer and Masson, 2002). The URG, about 40 km wide and 300 km long, extends form Basle in the south to just north of Strasbourg and is limited to the west by the Vosges and to the east by the Black Forest (Fig. 1). At the northern end of the URG, at a triple junction, the rift system splits up: one branch follows the Hessen depression (HG) and the Leine Graben (LG) and then apparently disappears beneath the young sediments of the North German Plain (Fig. 1). The other branch of the rift system, called the Lower Rhine Graben (LRG), which has been more active in recent times, continues northwestward through the Rheinish Massif into the Lower Rhine Embayment (LRE), changing orientation from N20°E to a NW-SE direction (Ziegler, 1992) (Fig. 1). Preceded by late Cretaceous volcanism, subsidence in the Rhine Graben started in its southern part under an extensional tectonic regime and occurred during two main phases begun in late Eocene and late Oligocene, respectively, and finished in the early Miocene (Villemin and Coletta, 1990). The Vosges–Black Forest doming during mid-Miocene was accompanied by volcanic activity within the graben proper and outside to the east, throughout the Cenozoic and again during the Quaternary in the Eifel area (Fig. 1). Subsidence ceased in the southern Rhine Graben due to a rotation of the maximum horizontal compressional stress from NNE–SSW to NNW–SSE about 20 Ma ago (Meier and Eisbacher, 1991; Glahn and Granet, 1992; Schumacher, 2002). Today, subsidence is present only in the northern part of the URG with rates of about −0.6 mm/year (Zippelt and Mälzer, 1981) and a maximum of −1 mm/year between Karlsruhe and Frankfurt (Ziegler, 1992). The southern end of the URG is characterized by small uplift and subsidence rates (Mälzer and Schlemmer, 1975; Zippelt and Mälzer, 1981), about +0.2 to −0.1 mm/year (Ziegler, 1992), not significant, (Rózsa et al., 2004; Schlatter et al., 2004) and by a quasi-compressive, strike-slip tectonic regime, with a maximum stress axes oriented NW–SE (Delouis et al., 1993). This tectonic regime changes to an extensional strike-slip and normal faulting type in the Rhenish Massif and in the LRG to the north, with the direction of the minimum stress axes NNE-SSW. The entire Rhine Graben system is seismically active and has been the locus of destructive earthquakes like which destroyed the city of Basle in 1356 (Meghraoui et al., 2001).

3. GPS data collection and strain field analysis

In order to reconstruct the deformation field in central western Europe we analysed results from GPS measurements carried out between 1996 and 2004. For this purpose we used the dataset of the velocities of permanent GPS stations in the ITRF2000 reference frame processed by Swisstopo (Swiss Federal Office of Topography, http://www.swisstopo.ch),

Table 2
Residuals of Helmert transformation expressed in mm/year for the three velocity components of the stations in common to the Swisstopo and EUREF datasets

Stations	RESx	RESy	RESz
BRST	0.03	0.16	0.44
GRAZ	0.24	0.35	0.19
KOSG	0.24	−0.16	−0.04
PADO	−0.23	0.27	−0.21
SJDV	0.32	−0.14	−0.35
TORI	−0.47	−0.19	−0.30
WTZR	−0.56	−0.42	0.30
ZIMM	0.39	0.08	−0.07

in the following called "Swisstopo dataset". The rates were determined for 55 GPS stations belonging to different networks, European Reference Frame (EUREF), Automated GPS Network for Switzerland (AGNES), Réseau GPS permanent dans les Alpes (REGAL) and Réseau GPS Permanent (RGP). The GPS sites are located in seven different countries (Italy, Switzerland, Austria, Germany, France, Belgium and The Netherlands), which cover the major structural units in central western Europe. The velocity results were obtained by Swisstopo on the basis of weekly solutions, calculated by processing the raw data with the Bernese software (Beutler et al., 2001; Brockmann et al., 2001, 2002a,b). The length of the time series varies within a range of 1–6 years (Table 1). Few stations, with unreliable values, or too short operation time, were excluded from the Swisstopo dataset. On the other hand, some ITRF2000 velocity values of EUREF stations (http://www.epncb.oma.be) (in the following called "EUREF dataset"), with long and stable time series, have been added, in order to increase the homogeneity of the GPS net. The new stations (BRUS, DELF, DRES, EIJS, GOPE, KOSG, OBE2, POTS, PTBB and WSRT) were integrated into the Swisstopo dataset through a Helmert transformation applied straight on to their geocentric velocity values (Tesauro et al., 2005).

The four parameters of the Helmert transformation (r_x, r_y, r_z and s) were estimated by least-squares adjustment at eight stations common in the two datasets (BRST, GRAZ, KOSG, PADO, SJDV, TORI, WTZR, ZIMM), chosen on the basis of their distribution in the area of study and on the data quality. The residuals obtained from the adjustment are displayed in Table 2. The Eurasian plate motion, calculated using a rotation rate of 0.260°/My around a pole located at 57.965° of latitude and −99.374° of longitude (Altamimi et al., 2002), was subtracted from the ITRF2000 velocities to estimate the residual velocities relative to Eurasia (Table 1 and Fig. 2).

We focused on the horizontal velocities only, because the uncertainties of vertical components are too large to allow reliable interpretations. The formal errors resulting from GPS data treatment are generally too small. Moreover, velocity estimation is performed through linear regression analysis leading to an error estimation which is proportional to (timespan)^(−3/2) for uncorrelated data series, which again is too optimistic. In order to reach a realistic upper bound for the errors of velocity, we adopted a (timespan)^(−1/2) law for the maximum error component.

Compared to the results obtained previously (Tesauro et al., 2005), we can observe that the GPS stations located between 4° and 16° of longitude are still moving in NW direction, but with slightly smaller rates, between 0.2 and 2.3 mm/year, with a velocity average of 1 mm/year (Table 1 and Fig. 2). Few GPS points differ from this general trend (Fig. 2), possibly because of local effects. The only two stations located within the URG area (KARL and STRA) show small velocities in N and NW direction (V_{abs} = 0.7 mm/year and 0.3 mm/year, respectively), according to Nocquet and Calais (2003) who predicted for this area movement of about 0.6 mm in NW direction. The stations located between −5° and 4° of longitude, move in WNW to SSW direction, with rates between 0.6 mm/year and 1.3 mm/year and a velocity average of 0.8 mm/year (Table 1 and Fig. 2). In contrast to this trend, BRST moves in NNW direction (Fig. 2), probably on account of more local than tectonic effect.

The strain rate field was obtained by interpolating the GPS results with least-squares collocation. This method implies the choice of a correlation function, which defines the interrelationship between different points observed (Straub, 1996; Kahle et al., 2000). Normally, the influence of a distant point should be smaller and the value of the function usually decreases with a growing distance and converges to zero. In our study we used a correlation length about equal to the average distance between the GPS stations (∼113 km). This choice comes from the consideration that if a correlation length is chosen too short the values observed remain isolated, while if it is too long, the field derived becomes extremely smooth. However, a correlation length should not be smaller than the average distance between the stations (Straub, 1996).

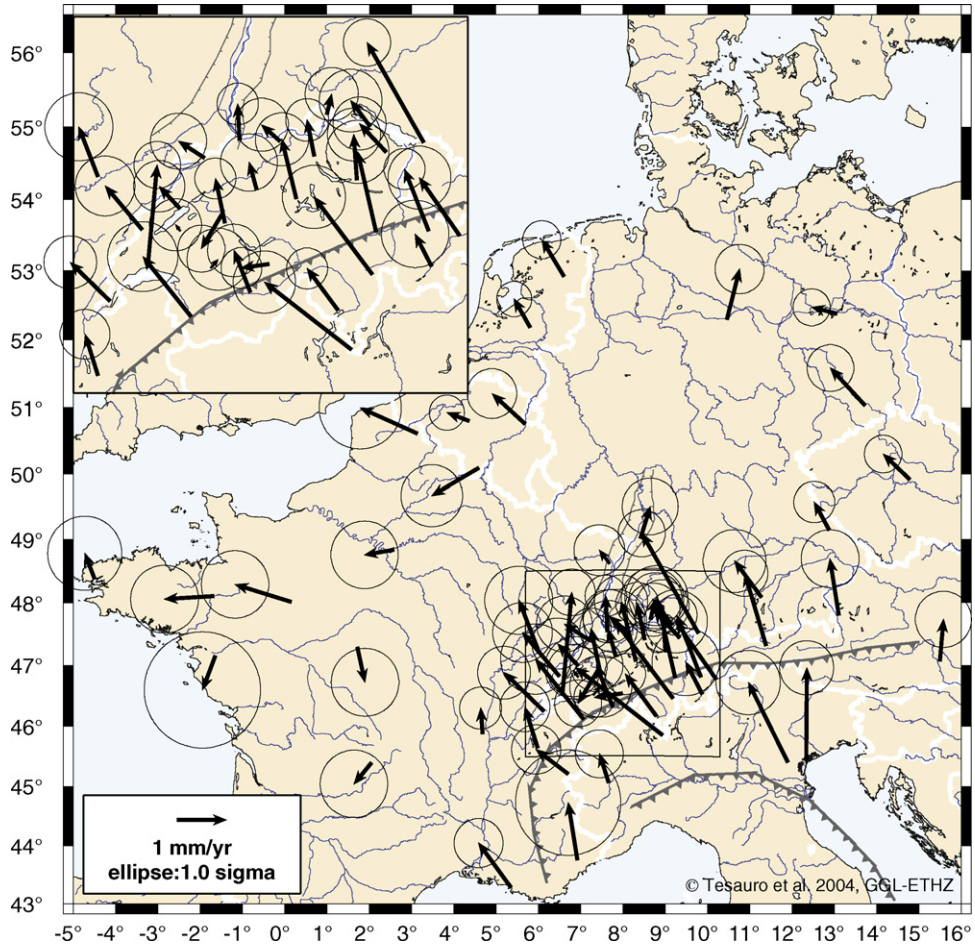

Fig. 2. Velocities relative to Eurasia for the time period 1996–2004. Euler pole values for the rotation of Eurasia: Lat = 57.965°, Long = −99.374°, $\omega = 0.260°$/My (Altamimi et al., 2002).

The principal axes of the 2D strain rate tensor and the corresponding dilatation rates are shown in Figs. 3 and 4. We can observe that most of the strain is concentrated in the central part of the Alps and in the Molasse Basin, the foreland of the Alps (Figs. 1, 3 and 4). More precisely, we found relatively high values of compression in Switzerland and in southwestern Germany, up to 7 ± 2 nstrain/year, oriented NW-SE (Figs. 3 and 4). Low values of extension are found in Belgium and in France between the Armorican Massif and the Massif Central, with a maximum value of 4 ± 2 nstrain/year (Figs. 3 and 4). In the Rhine Graben area the deformation rates are within the margin of error (of the order of 4 nstrain/year). Moreover, we calculated the normal and the shear components of the strain rate tensor perpendicular and parallel to the Alpine boundary and to the eastern and western Rhine Graben borders. The results are very similar to the previous ones (Tesauro et al., 2005): relatively significant compressional strain rates were found perpendicular to the central part of the Alpine boundary and dextral shear strain rate along the central part of the Alps. Both borders of the Rhine Graben show insignificant values of normal and shear strain rates.

We can observe that with 1 year more of input data (Tesauro et al., 2005) the stations located in the western part of the area of study are affected by a more pronounced change in the direction of the movement. In particular, we can observe that LILL, MANS and RENN stations registered the largest differences between the current (WNW) (Table 1 and Fig. 2) and the previous (SSW) directions (Tesauro et al., 2005). However, these rotations of the velocity vectors might be only an effect of short time spans (Table 1). On the other hand, the strain rates in central western Europe are slightly smaller, and the most evident results are the orientation of the compressional strain rate axes, mostly NW-SE and its rotation to N-S, NNE-SSW in the Molasse Basin (Figs. 1 and 3). These data are better constrained than the previous ones (Tesauro et al., 2005), on account of the longer periods analysed and of the increased number of GPS

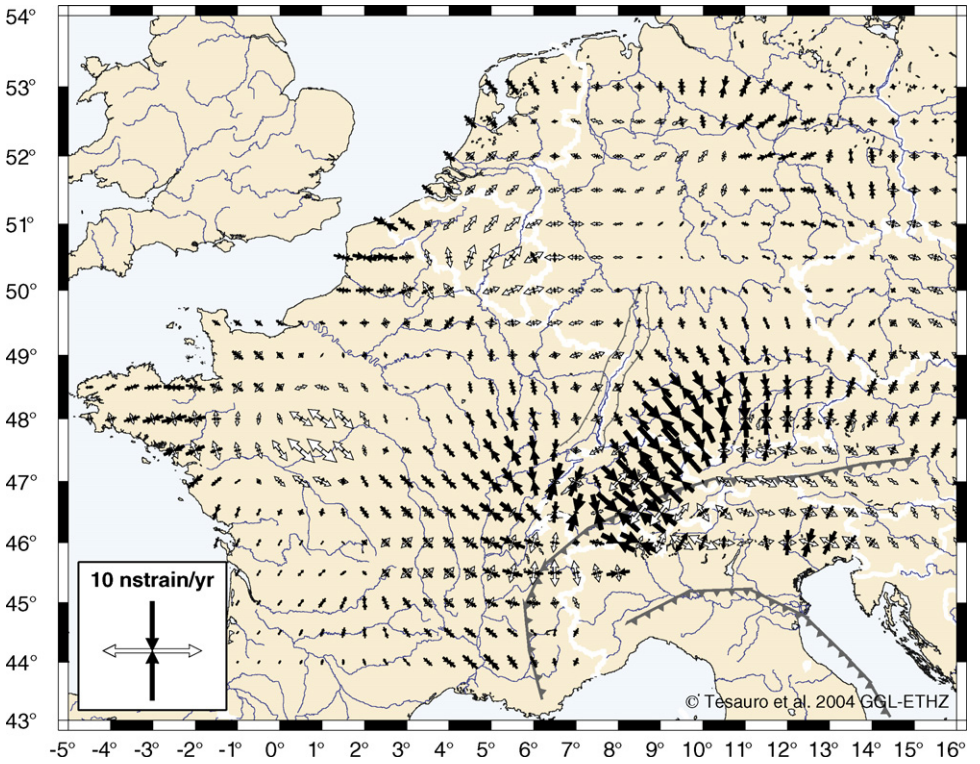

Fig. 3. Principal axes and values of the strain rate tensor obtained by the least-squares collocation. Covariance distance: 113 km, sigma of signal: 0.76 mm/year. Compressional and extensional axes are in black and in white, respectively. The formal errors are of the order of 4 nstrain/year.

stations (DOUR, DELF, DRES, EIJS, OBE2, PTBB, SBGZ) especially in the northern part of the area of study. On the other hand, in the LRG and in France the density of the GPS net remains too low to measure precisely the deformation present there.

4. Seismicity in central western Europe

Central western Europe is characterized by diffuse seismicity with earthquake magnitudes rarely exceeding 4.0, that can be attributed to the existence of old zones of weakness, which are reactivated under the current stress field (Ziegler, 1992). Many earthquakes occur in the shallow crust (within 15 km), while few of them with epicenters mostly located in the Molasse Basin (Fig. 1), reach the Moho depth (about 30 km) (Kastrup, 2002; Kastrup et al., 2004; Delacou et al., 2004) and have been interpreted as indicator of high fluid pressure (Deichmann, 1992). Looking at the distribution of seismicity in central western Europe (Fig. 5), we can observe that most of the earthquakes are concentrated preferentially along three bends: the Alpine chain, the ECRIS and the zone between the Armorican Massif and the Massif Central, two segments of the Hercynian Orogeny (400–250 My), dividing the Paris Basin in the north from the Aquitaine Basin in the south (Fig. 1).

In order to evaluate the amplitude of the seismic strain rates we used the Kostrov (1974) estimate:

$$\dot{\varepsilon} = \frac{1}{2\mu VT} \sum M_0 \tag{1}$$

where μ is the shear modulus of the brittle crust, V the cell volume elastically deformed (grid area times the seismogenic thickness), T the time period of the earthquake record and M_0 the seismic moment. According to Jackson et al. (1992) the grid area into which the deforming zone is divided should be large enough to satisfy the assumptions implicit in Kostrov's method. In fact, for Kostrov summation grid cells should delimit areas of homogeneous tectonic deformation (Jenny et al., 2004). This condition is verified if they are larger than the size of the largest faults they contain (Jackson et al., 1992). In our area of study, where strong earthquakes are seldom, we chose a cell grid of 0.5° (∼55 km). The

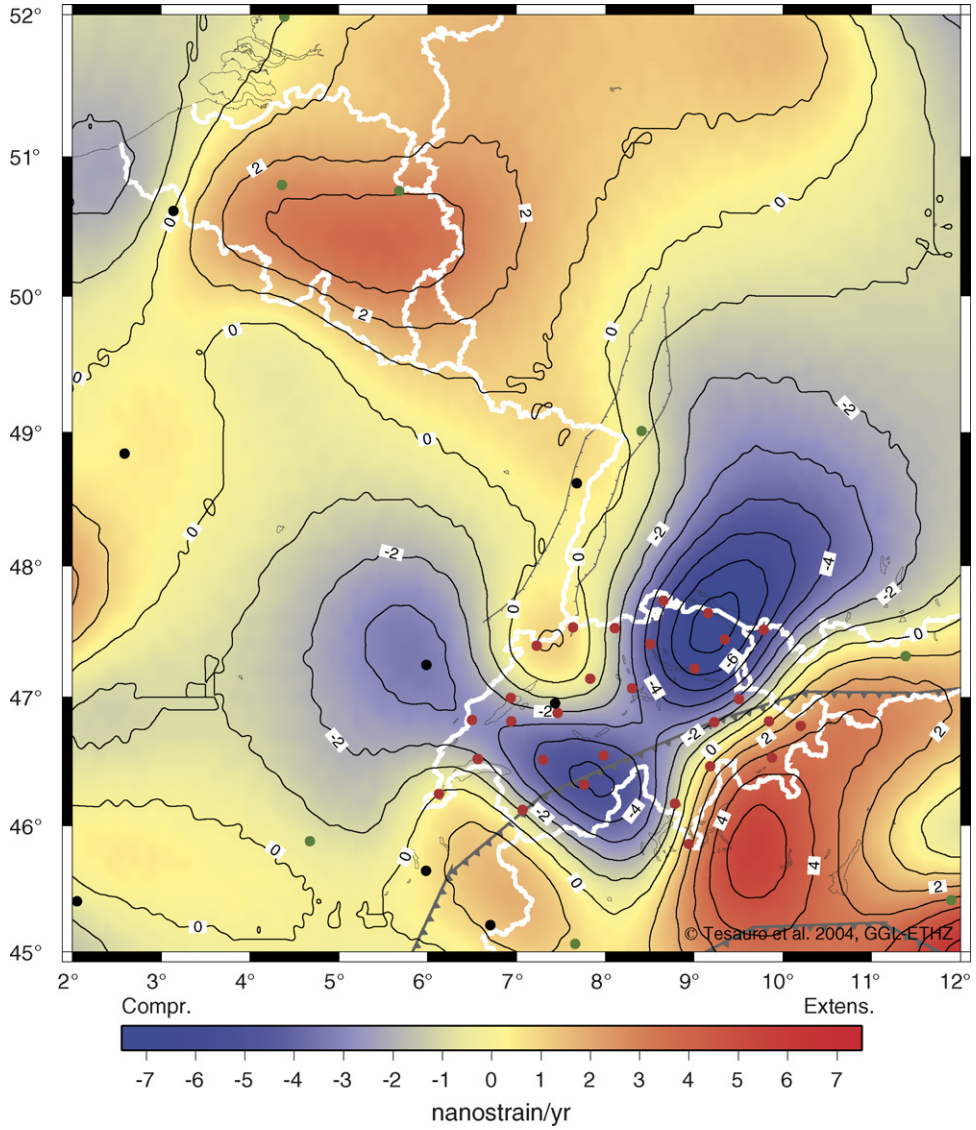

Fig. 4. Two-dimensional dilatation rates in central western Europe calculated from the trace of the 2D strain rates tensor ($\varepsilon_1 + \varepsilon_2$). Covariance distance: 113 km, sigma of signal: 0.76 mm/year. Red, green and black dots represent GPS permanent stations of the AGNES, EUREF and REGAL-RGP networks, respectively. The formal errors are between 5 and 6 nstrain/year.

use of a coarser grid would be not justified, while a finer grid would not satisfy the assumptions implicit in the Kostrov summation everywhere. However, the use of a different grid (coarser or finer) would produce a change in the amplitude of the seismic strain rates (in particular, the data values would show larger and more rapid fluctuations for finer than for coarser grid), but would not affect much its distribution between the geological realms. We assumed a seismogenic thickness of 15 km, since more than the 90% of the earthquakes occur within this depth. Furthermore, μ is taken equal to $3.0 \times 10^{10}\,\mathrm{Nm}^{-2}$, a commonly used average for the seismogenetic upper crust (Anderson and Jackson, 1987; Holt et al., 1991; Jackson et al., 1992; Koravos et al., 2003). The seismic moment M_0 in Nm is related to the earthquakes magnitude M, by the following equation (Kagan, 1997):

$$M = \tfrac{2}{3} \log\, M_0 - 6.03 \tag{2}$$

To calculate M_0 we referred to the instrumental seismic catalogue, coming from the National Earthquake Information Center (NEIC). The NEIC catalogue used covers the time period between the 1st of January 1973 and the 30th of

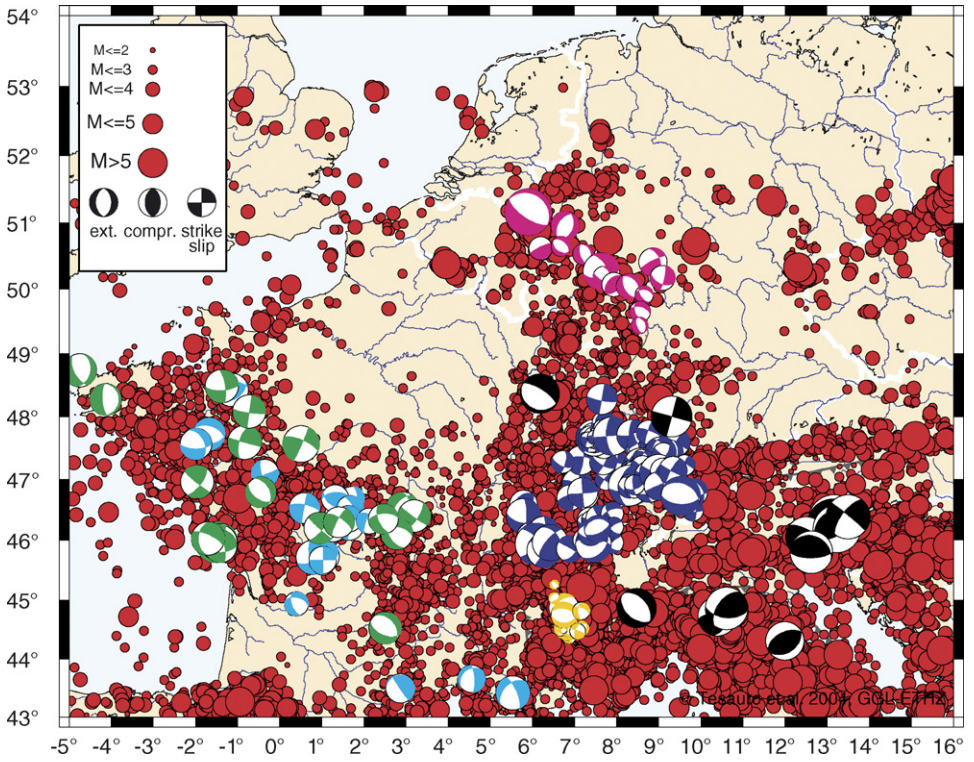

Fig. 5. Earthquakes in central western Europe since 1973 from the National Earthquake Information Center (NEIC) and fault plane solutions (FPS) since 1961 from Plenefisch and Bonjer (1997) (in violet), Kastrup (2002) (in blue), Sue et al. (1999) (in yellow), Nicolas et al. (1990) (in turquoise), Delouis et al. (1993) (in green) and Harvard CMT Catalog (in black).

June 2004 and contains 41173 events with magnitude between 1.0 and 6.5 within the area of study. The catalogue uses several magnitude scales, among them *mb* and *Ms* are provided for most of the moderate and large events. For the sake of simplicity, we assumed that the different magnitudes used, with a tolerance of 0.2, are equivalent (Anderson and Jackson, 1987). However, the magnitude errors are expected to be small in comparison to errors of the estimated strain rate field. In order to test the completeness of NEIC catalogue, we plotted the time distribution of earthquake numbers for each magnitude class (Fig. 6), according to previous authors (Mulargia et al., 1987; Kagan, 1997; Jenny et al., 2004). We can observe from Fig. 6 that the curves for M between 3.0 and 4.4 exhibit a sudden increase of seismicity since 1984, indicating a great undersampling until this date. On the other hand, similar curves for $M \geq 4.5$ are reasonably uniform in time. Such a comparison indicates that the catalogue might be incomplete for $M \leq 4.4$. Therefore, we carried out our analysis using magnitude thresholds of 3.0 and of 4.5 for the events, which have occurred since 1984 and 1973, respectively. In this way, we used 8999 events of the original catalogue and we included the significant contribution that the small earthquakes ($M \leq 4.4$) can give to the seismic moment values. Therefore, according to Eq. (2), we calculated the average strain rates as:

$$\dot{\varepsilon} = \frac{1}{2\mu V} \sum \left(\frac{M_{0_{(M \leq 4.4)}}}{T_{(1984-2004)}} + \frac{M_{0_{(M \geq 4.5)}}}{T_{(1973-2004)}} \right) \tag{3}$$

It should be noted that the poorly constrained parameter values of the Kostrov estimate and the inhomogeneous distribution of the GPS stations do not allow us to discuss quantitatively the difference existing between the seismic and the geodetic strain rates. However, we could display and analyse the seismic strain rates distribution in the different regions of the area of study. Fig. 7 shows that about 50% of central western Europe is not seismically active, and is characterized by strain rates less than 10^{-3} nstrain/year. These regions correspond mostly to the Aquitaine Basin, the Paris Basin and the German Plain. Relatively low deformation rates, up to 1 nstrain/year, are measured in the Massif Central, in the Armorican Massif, in the zone in between, in the LRE and in the North Sea. The highest values of seismic strain rates ($\dot{\varepsilon} \geq 10$ nstrain/year) are detected in the central and in the northeastern part of Italy along the

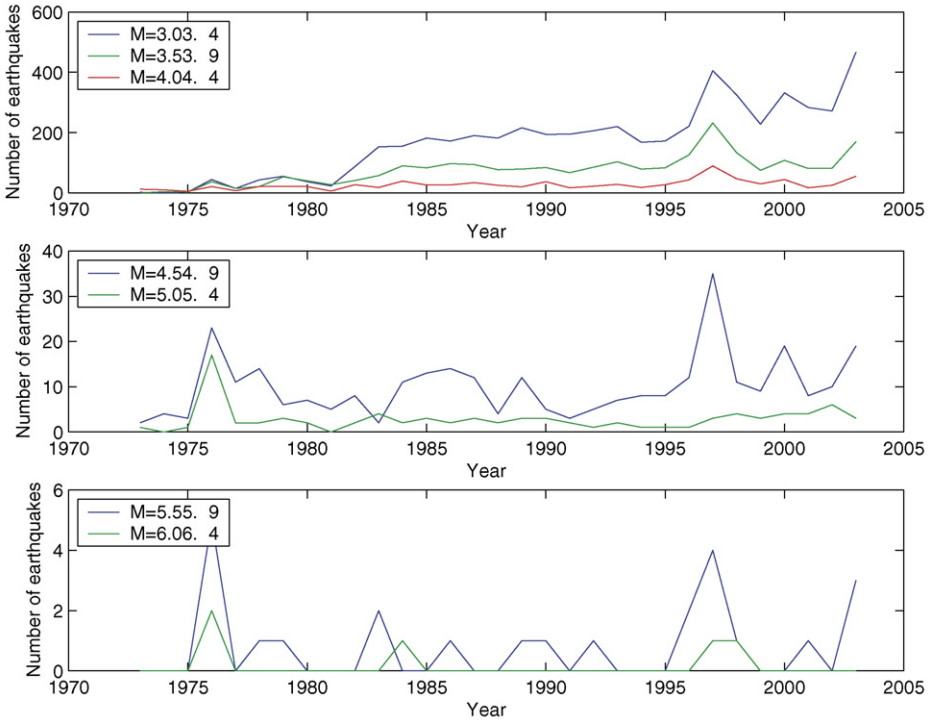

Fig. 6. Time distribution of earthquake numbers for different classes of magnitude.

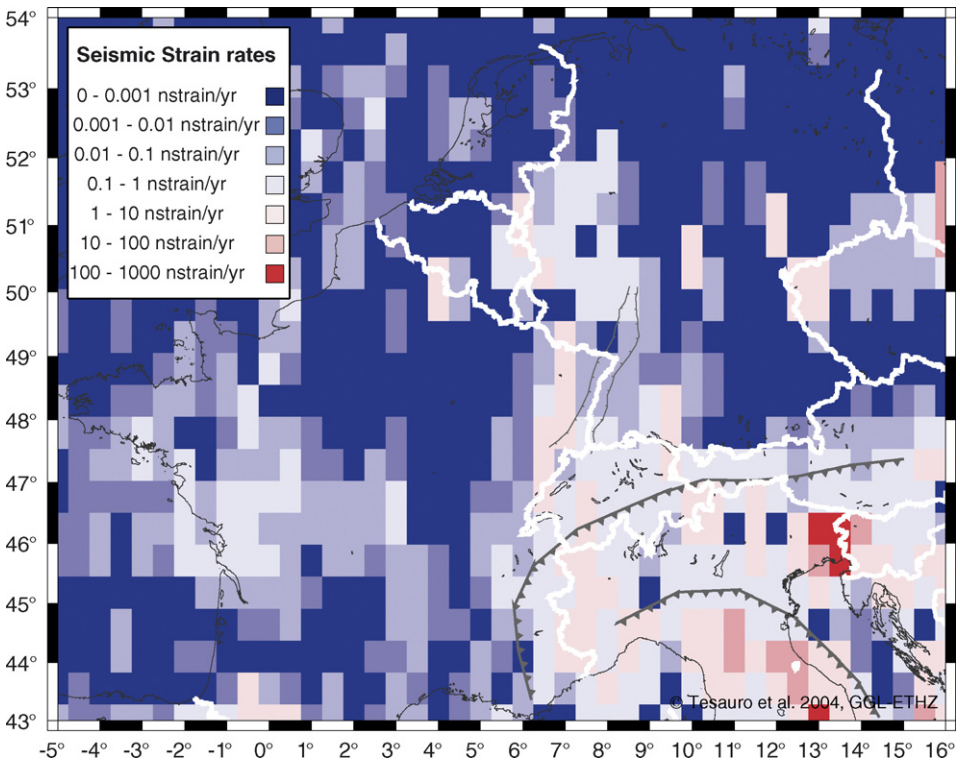

Fig. 7. Seismic strain rates distribution in central western Europe. The highest values of deformation rates ($\dot{\varepsilon} > 10$ nstrain/year) are found in the Appenninic chain and in the eastern part of the Alps, while relative high values, up to 10 nstrain/year, are measured prevalently along the Alpine belt and the ECRIS.

Slovenian border, corresponding to the Apennine chain and the area of convergence of the Adria block, respectively. The Alps are characterized by relatively high strain rates, of up to 10 nstrain/year, especially in northern part of Italy, along the France and the Austrian border and in western Switzerland. Relatively high values of strain rates (up to 10 nstrain/year) are detected also in the south part of the URG, in the Vosges, in the Jura, in the Rhenish Massif, and in the Bohemian Massif. In contrast to the geodetic strain rates, which are higher concentrated in the central part of the Alps and in the Molasse Basin (Figs. 3 and 4), the seismic strain rates are more scattered in the area of study (Fig. 7). However, for the reasons discussed before, we cannot make a quantitative evaluation of the percentage of the seismic and aseismic deformation.

From the focal mechanisms displayed in Fig. 5 we can observe that in central western Europe the predominant deformation regime is strike-slip; however, normal faulting regimes are also widely distributed and dominant in certain areas. In these areas the change in the tectonic style occurs on a short scale, over distances of several tens to hundreds of kilometers, in contrast to other continental areas (e.g. the eastern north America stress province), which shows a smoother transition of the tectonic regime (Müller et al., 1997). For instance, in France regimes vary from normal faulting in the Rhône graben and the southern Massif Central to a mixed mode of normal faulting and strike-slip northwest of the Massif Central (Müller et al., 1992) (Figs. 5 and 1). Another example is the Rhine Graben System that is characterized prevalently by normal faulting regime in the northern part (the LRG) and a strike-slip regime in the southern part (the URG) (Figs. 5 and 1). Ahorner (1975) already recognized this difference in the tectonic style and its concordance with the same horizontal compressional strain axes.

We used the focal mechanisms available for the area of study (Fig. 5) to estimate the style of the seismic deformation. For a better visualization, we averaged the seismic moment tensors of the events located in the same half degree of

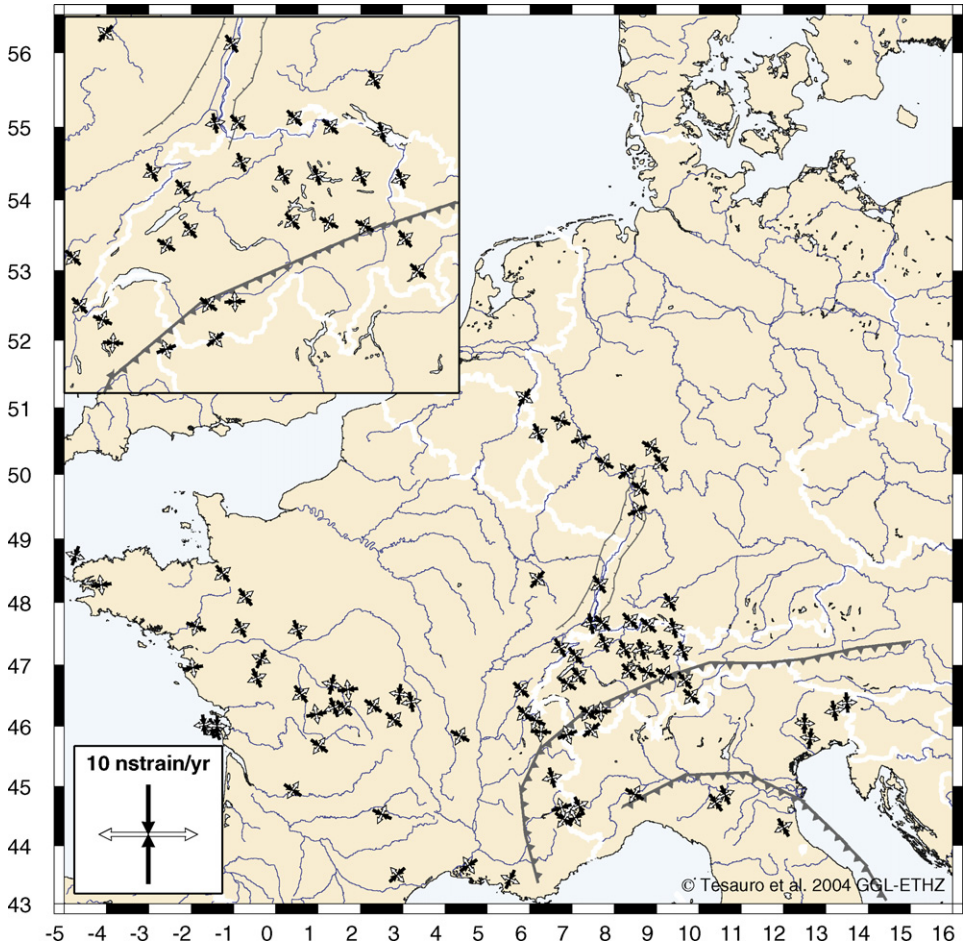

Fig. 8. Directions of the seismic strain axes. Compressional and extensional axes are in black and in white, respectively.

latitude and longitude and we displayed the resulted strain rates in the middle point of the cell. When a single event was found in a grid cell, the corresponding strain rates are displayed where the same event is located (Fig. 8). We can observe that despite the not homogeneous space distribution of the data, they show a quite uniform pattern, with the compressional strain axes mostly NW-SE oriented. The same axes show a clockwise rotation along the Alpine arc: the roughly NNW-SSE directed compression in the central part of the Alpine chain becomes N-S in the southeastern part of the Alps (Fig. 8). This fan-like pattern of the strain axes, first observed by Pavoni (1980), can be related to the ongoing convergence of the African and Eurasian plates. We can observe that the deformation style reconstructed with the GPS solutions is quite in agreement with that showed by the FPS, except for the small misfit found in the western part of France, where the geodetic and the seismic compressional strain axes are NE-SW and NW-SE oriented, respectively (Figs. 3 and 8). However, in this area the limited coverage of the GPS stations and of the number of the FPS do not allow a comparison between the style of the geodetic and the seismic deformation. Moreover, sometimes, this kind of comparison is difficult to do, despite the amount of data available, since intraplate earthquakes tend to occur on pre-existing weak zones. Therefore, strain directions inferred from individual mechanisms may reflect the orientations of such features, rather than regional tectonic strain (Wiens and Stein, 1985; Coblentz et al., 1995).

5. Discussion

The GPS results have shown that central western Europe is characterized by small movements, within 2.4 mm/year relative to Eurasia (Table 1 and Fig. 2), producing relatively low compressional and extensional strain rates (Figs. 3 and 4). In particular, these results predict compression in the Alpine area, with a maximum value of 6.5 ± 2 nstrain/year in the Molasse Basin. The orientation of the compressional strain axes is NW-SE in the central part of the Alps, while a small rotation of the same axes to NNE-SSW direction is found in the eastern part of the chain and in the Molasse Basin east to the URG (Figs. 1 and 3). The results are in agreement with the seismic data (Figs. 5 and 8), showing a counterclockwise rotation of the compressional axes from NW-SE to NNE-SSW along the Alpine chain, and with which obtained by previous authors (Pavoni, 1980; Bassi et al., 1997; Bada et al., 1998; Grenerczy et al., 2000). The orientation of the compressional strain axes, generally NW-SE and NNE-SSW in the western and eastern part of the area, respectively, can be explained largely as a function of compressive plate boundary forces and of the geometry of the plate boundaries that these forces act on (Müller et al., 1992; Grünthal and Stromeyer, 1992). Furthermore, this area is characterized by relative high seismic strain rates, especially the eastern part of the Alps (Fig. 7), possibly related to the convergence of the Adria block.

The GPS data do not reveal the extension found in the western part of the Alps by previous authors (Eva et al., 1997; Maurer et al., 1997; Eva and Solarino, 1998; Sue et al., 1999; Calais et al., 2000, 2002; Baroux et al., 2001; Vigny et al., 2002; Kastrup, 2002; Sue and Tricart, 2003; Delacou et al., 2004; Kastrup et al., 2004). On the other hand, our study is on a regional scale, while to detect this local extension a higher number of GPS permanent stations and longer time series are needed. The extensional tectonic regime in the western Alps is correlated with the zones of high crustal thickness (characterized by high large-scale topography and strong negative Bouguer anomalies) and can be controlled by internal gravitational forces (Delacou et al., 2004). Recent studies (Kastrup, 2002; Kastrup et al., 2004) have observed a difference in the deformation style between the foreland of the Alpine chain and the Alps. In particular, they found an increase of the proportion of normal faulting to the south in the highest and compressional parts of the Alps (Fig. 5). Furthermore, these data show also evidence for a systematic counterclockwise rotation of the horizontal deformation from east to west in the Alpine foreland and from north to south across the Alps (Fig. 5). Kastrup et al. (2004) interpret them as a superimposition of a local tensional stress, related to spreading effects within the orogen, and the regional compressive stress, induced by the Atlantic ridge push and on African–Eurasian plates convergence. The tensile nature and the orientation of this strain can be the result of lateral density changes due to the crustal roots (Sue et al., 1999; Kastrup, 2002; Sue and Tricart, 2003; Kastrup et al., 2004). However, the Alps seem to locally influence the strain pattern within the orogen proper (Delacou et al., 2004), without seriously affecting the strain field of Europe as a whole (Müller et al., 1992).

Along the ECRIS, from the south to the north part, relative high values of seismic strain rates are found (up to 10 nstrain/year, Fig. 7), while GPS data show a transition from a compressional to an extensional tectonic regime, with the compressional strain axes NW-SE oriented. These results are consistent with which achieved in previous studies, which predict a change in the tectonic style in the region where the Rhine Graben system varies its orientation from

SW-NE to SE-NW direction (Ahorner, 1975; Larroque et al., 1987; Larroque and Laurent, 1988; Müller et al., 1992; Delouis et al., 1993; Bonjer, 1997; Plenefisch and Bonjer, 1997; Schumacher, 2002; Behrmann et al., 2003; Giamboni et al., 2004; Tesauro et al., 2005; Ziegler and Dèzes, 2004). This tectonic regime variation, visible also from the FPS (Fig. 5), highlights the difference in the evolution between the northern and the southern part of the Rhine Graben system (Glahn and Granet, 1992; Villemin et al., 1986).

In the zone that connects the Armorican Massif to the Massif Central negligible seismic strain rates are found (Fig. 7). GPS data show relatively high extension (4 nstrain/year) (Fig. 3), according to the strike-slip tensional regime predicted from the FPS (Nicolas et al., 1990; Delouis et al., 1993) (Fig. 5). In the same area we can observe the small difference in the direction of the compressional strain axes obtained from the GPS data (NE-SW oriented) (Fig. 3) and from the FPS (NW-SE) (Fig. 8). It is noted that in this area a fair comparison between the style of the geodetic and the seismic strain direction is hard to do on account of the limited number of GPS permanent stations.

The regional change in the tectonic style observed in central western Europe has been discussed by many authors and can be linked to: (a) variation in the force along the southern European boundary, due to irregular shape of the colliding continental margins (Illies, 1975; Regenauer-Lieb and Petit, 1997), (b) variation in the lithosphere strength of thermal origin (Grünthal and Stromeyer, 1992; Müller et al., 1997), (c) mechanical decoupling between crust and lithospheric mantle, allowing crustal fragments to move independently of each other (Müller et al., 1997; Garcia-Castellanos et al., 2000). On the other hand, tomography studies (Granet et al., 1995a; Marquering and Sneider, 1996; Bijwaard et al., 1998) showed significant velocity variations under central western Europe. More precisely, low velocity anomalies of *P* and *S* waves were found under the Rhenish Massif and the Massif Central, while high velocity anomalies associated with subduction were observed under the Alps (Goes et al., 2000a,b). Goes et al. (2000a) inverted the shallow upper mantle *P* and *S* wave velocities under Europe for temperature, assuming that seismic velocity anomalies could be solely attributed to variations in temperature. Their results confirm the presence of thermal anomalies in the European mantle lithosphere. They found temperatures under the Massif Central and the Rhenish Massif at a depth of 50 km 100–300° higher than for the surrounding areas. These mantle thermal anomalies are consistent with the presence of a plume (Granet et al., 1995b; Sobolev et al., 1997; Zeyen et al., 1997; Goes et al., 2000a,b; Ritter et al., 2001), that likely was the driving force of the volcanic activity which occurred there in the past (Granet et al., 1995b).

6. Conclusions

This regional study represents a good starting point for more detailed research works in the future. More GPS stations and longer time series are needed in order to better constrain the relatively small deformation rates in this area, finding more connections with the tectonic history and evolution of the geological features.

Despite the inhomogeneous coverage of the GPS net, the shortness of the time series and of the seismic catalogue, we have shown that:

- The area of maximum deformation is localized along the Alpine chain.
- There is a transition from a compressional to an extensional regime along the ECRIS which is concordant with previous works.
- The directions of the principal axes of the seismic and geodetic strain rates are in good agreement in most parts of the area of study.
- Plate boundary forces and anomalous mantle structures under central western Europe appear to play a role in the tectonic activity of this area.

Acknowledgements

We would like to thank Saskia Goes of the Geophysics Department of ETH of Zürich for helpful discussions on determining seismic strain. Valuable comments of two anonymous reviewers improved the quality of the manuscript. Funds were kindly provided by EU grant HPRN-2000-00053 (Swiss Federal Office of Science and Education, BBW N_0. 99-0567-2) in the frame of the project ENTEC.

References

Achauer, U., Masson, F., 2002. Seismic tomography of continental rifts revisited: from relative to absolute heterogeneities. Tectonophysics 358, 17–37.

Ahorner, L., 1975. Present-day stress field and seismotectonic block movements along major fault zones in central Europe. Tectonophysics 29, 233–249.

Altamimi, Z., Sillard, P., Boucher, C., 2002. ITRF2000: a new release of the International Terrestrial Reference Frame for earth science applications. J. Geophys. Res. 107 (B10), 2214, doi:10.1029/2001JB000561.

Anderson, H., Jackson, J.A., 1987. Active tectonics of the Adriatic region. Geophys. J. R. Astr. Soc. 91, 937–983.

Bada, G., Cloetingh, S., Gerner, P., Horvath, F., 1998. Sources of recent tectonic stress in the Pannonian region: inferences from finite element modeling. Geophys. J. Int. 91, 937–983.

Baroux, E., Bethoux, N., Bellier, O., 2001. Analyses of the stress field in southeastern France from earthquake focal mechanisms. Geophys. J. Int. 145, 336–348.

Bassi, G., Sabadini, R., Rebaï, S., 1997. Modern Tectonic regime in the Tyrrenian area: observations and models. Geophys. J. Int. 129, 330–346.

Becker, A., 1999. In situ stress data from the Jura Mountains—new results and interpretation. Terra Nova 11, 9–15.

Behrmann, J.H., Hermann, O., Horstmann, M., Tanner, D.C., Bertrand, G., 2003. Anatomy and kinematics of oblique continental rifting revealed: a three-dimensional case study of the southeast Upper Rhine graben (Germany). AAPG Bull. 87 (7), 1105–1121.

Beutler, G., Bock, H., Brockmann, E., Dach, P., Fridez, P., Gurtner, W., Hugentobler, U., Ineichen, D., Johnson, J., Meindl, M., Mervart, L., Rothacher, M., Schaer, S., Springer, T., Weber, R., 2001. In: Hugentobler, U., Schaer, S., Fridez, P. (Eds.), Bernese GPS Software Version 4.2. Astronomical Institute, University of Berne.

Bijwaard, H., Spakman, W., Engdahl, E.R., 1998. Closing the gap between regional and global travel time tomography. J. Geophys. Res. 103, 30055–30078.

Bonjer, K.-P., 1997. Seismicity pattern and style of seismic faulting at the eastern borderfault of the southern Rhine Graben. Tectonophysics 275, 41–69.

Brockmann, E., Grünig, S., Schneider, D., Wiget, A., Wild, U., 2001. In: Torres, J.A., Hornik, H. (Eds.), Introduction and First appLications of a Real Time Precise Positioning Service Using the Swiss Permanent Network 'AGNES'. National Report of Switzerland. Subcommission for the European Reference Frame (EUREF), Dubrovnik.

Brockmann, E., Hug, R., Signer, T., 2002a. In: Torres, J.A., Hornik, H. (Eds.), Geotectonics in the Swiss Alps using GPS. Subcommission for the European Reference Frame (EUREF). EUREF Publication 11.

Brockmann, E., Grünig, S., Schneider, D., Wiget, A., Wild, U., 2002b. Applications of the Real-Time Swiss GPS Permanent Network AGNES. In: Proceedings of the EGS XXVII General Assembly Nice, 21–26 April 2002, Session 9 on Evolving Space Geodesy Techniques, Physics and Chemistry of the Earth.

Calais, E., 1999. Continuous GPS measurements across the western Alps, 1996–1998. Geophys. J. Int. 138 (1), 221–230.

Calais, E., Gallison, L., Stéphan, J.-F., Delteil, J., Deverchere, J., Larroque, C., de Lepinay, Mercier, Popoff, M., Sosson, M., 2000. Crustal strain in the Southern Alps, France, 1948–1998. Tectonophysics 319, 1–17.

Calais, E., Nocquet, J.-M., Jouanne, F., Tardy, M., 2002. Current strain regime in the Western Alps from continuous Global Positioning System measurements, 1996–2001. Geology 30 (7), 651–654.

Coblentz, D.D., Sandiford, M., Richardson, R.M., Zhou, S., 1995. The origins of the intraplate stress field in continental Australia. Earth Planet. Sci. Lett. 133, 299–309.

Deichmann, N., 1992. Structural and rheological implications of lowercrustal earthquakes below northern Switzerland. Phys. Earth Planet. Int. 69, 270–280.

Delacou, B., Sue, Ch., Champagnac, J.D., Burkhard, M., 2004. Present-day geodynamics in the bend of the western and central Alps as constrained by earthquake analysis. Geophys. J. Int. 158, 753–774.

Delouis, B., Haessler, H., Cisternas, A., Rivera, L., 1993. Stress tensor determination in France and neighbouring regions. Tectonophysics 221, 413–438.

DeMets, C., Gordon, R.G., Argus, D.F., Stein, S., 1994. Effect of recent revisions to the geomagnetic reversal time scale on estimates of current plate motions. Geophys. Res. Lett. 21 (20), 2191–2194.

Eva, E., Solarino, S., Eva, C., Neri, G., 1997. Stress tensor orientation derived from fault plane solutions in the southwestern Alps. J. Geophys. Res. 102 (B4), 8171–8185.

Eva, E., Solarino, S., 1998. Variations of stress directions in the western Alpine arc. Geophys. J. Int. 135, 438–448.

Garcia-Castellanos, D., Cloetingh, S., Van Balen, R., 2000. Modelling the middle Pleistocene uplift in the Ardennes–Rhenish Massif: thermo-mechanical weakening under the Eifel? Global Planet. Change 27, 39–52.

Giamboni, M., Ustaszewski, K., Schmid, S.M., Schumacher, M.E., Wetzel, A., 2004. Plio-Pleistocene transpressional reactivation of Paleozoic and Paleogene structures in the Rhine-Bresse transform zone (northern Switzerland and eastern France). Int. J. Earth Sci. 93 (2), 207–223.

Glahn, A., Granet, M., 1992. 3-D structure of the lithosphere beneath the southern Rhine Graben area. Tectonophysics 208, 149–158.

Goes, S., Govers, R., Vacher, P., 2000a. Shallow mantle temperatures under Europe from P and S wave tomography. J. Geophys. Res. 105 (B5), 11153–11169.

Goes, S., Loohuis, J.J.P., Wortel, M.J.R., Govers, R., 2000b. The effect of plate stress and shallow mantle temperatures on tectonics of northwestern Europe. Global Planet. Change 27, 23–38.

Granet, M., Stoll, G., Dorel, J., Achauer, U., Poupinet, G., Fuchs, K., 1995a. The Massif Central (France). New constraints on the geodynamical evolution from teleseismic tomography. Geophys. J. Int. 121, 33–48.

Granet, M., Wilson, M., Achauer, U., 1995b. Imaging a mantle plume beneath the Massif Central (France). Earth Planet. Sci. Lett. 136, 281–296.

Grenerczy, G., Kenyeres, A., Fejes, I., 2000. Present crustal movement and strain distribution in Central Europe inferred from GPS measurements. J. Geophys. Res. 105 (B9), 21835–21846.

Grünthal, G., Stromeyer, D., 1992. The recent crustal stress field in central Europe: trajectories and finite element modelling. J. Geophys. Res. 97, 11,805–11,820.

Holt, W.E., Wallace, J.F.N.T., Haines, A.J., 1991. The active tectonics of the eastern Himalayan syntaxis and surrounding regions. J. Geophys. Res. 96 (B9), 14,595–14,632.

Illies, J.H., 1975. Recent and paleo-intraplate tectonics in stable Europe and the Rhinegraben rift system. Tectonophysics 29, 251–264.

Jackson, J.A., Haines, J., Holt, W., 1992. The horizontal velocity field in the deforming Aegean Sea region determined from the moment tensor of the earthquakes. J. Geophys. Res. 97 (B12), 17657–17684.

Jenny, S., Goes, S., Giardini, D., Kahle, H.-G., 2004. Earthquake recurrence parameters from seismic and geodetic strain rates in the eastern Mediterranean. Geophys. J. Int. 157, 1331–1347.

Kagan, Y.Y., 1997. Seismic-moment frequency relation for shallow earthquakes: regional comparison. J. Geophys. Res. 102 (B2), 2835–2852.

Kahle, H.-G., Cocard, M., Peter, Y., Geiger, A., Reilinger, R., Barka, A., Veis, G., 2000. GPS-derived strain field within the boundary zones of the Eurasian, African, and Arabian Plates. J. Geophys. Res. 105 (B10), 23,353–23,370.

Kastrup, U., 2002. Seismotectonics and Stress Field Variations in Switzerland. PhD Dissertation. ETH Zürich.

Kastrup, U., Zoback, M.L., Deichmann, N., Evans, K.F., Giardini, D., Andrew, J.M., 2004. Stress field variations in the Swiss Alps and the northern Alpine foreland derived from inversion of fault plane solutions. J. Geophys. Res. 109, B01402 doi:10.1029/2003JB002550.

Koravos, G.Ch., Main, I.G., Tsapanos, T.M.R., Musson, M.W., 2003. Maximum earthquake magnitudes in the Aegean area constrained by tectonic moment release rates. Geophys. J. Int. 152, 94–112.

Kostrov, V.V., 1974. Seismic moment and energy of earthquakes, and seismic flow of rocks. Izv. Acad. Sci. USSR Phys. Solid Earth 1, 23–44, Engl. Trans.

Larroque, J.M., Etchecopar, A., Philip, H., 1987. Evidence for the permutation of stresses σ_1 and σ_2 in the Alpine foreland: the example of the Rhine Graben. Tectonophysics 144, 315–322.

Larroque, J.M., Laurent, Ph., 1988. Evolution of the stress field pattern in the south of the Rhine Graben from the Eocene to the present. Tectonophysics 148, 41–58.

Mälzer, H., Schlemmer, H., 1975. Geodetic measurements and recent crustal movements in the southern upper Rhinegraben. Tectonophysics 29, 275–282.

Marquering, H., Sneider, R., 1996. Shear-wave velocity structure beneath Europe, the northeastern Atlantic and western Asia from waveform inversions including surface-wave mode coupling. Geophys. J. Int. 127, 283–304.

Maurer, H., Burkhard, M., Deichmann, N., Green, G., 1997. Active tectonism in the central Alps: contrasting stress regimes north and south of the Rhone Valley. Terra Nova 9, 91–94.

Meghraoui, M., Delouis, B., Ferry, M., Giardini, D., Huggenberger, P., Spottke, I., Granet, M., 2001. Active normal faulting in the upper Rhine Graben and Paleoseismic identification of the 1356 basel earthquake. Science 293, 2070–2073.

Meier, L., Eisbacher, G.H., 1991. Crustal kinematics and deep structure of the northern Rhine Graben, Germany. Tectonics 10 (3), 621–630.

Meyer, B., Lacassin, R., Brulhet, J., Mouroux, B., 1994. The Basel 1356 earthquake: which fault produced it? Terra Nova 6, 54–63.

Mulargia, F., Broccio, F., Achilli, V., Baldi, P., 1987. Evaluation of aseismic quiescence pattern in southeastern Sicily. Tectonophysics 116, 335–364.

Müller, B., Zoback, M.L., Fuchs, K., Mastin, L., Grgersen, S., Pavoni, N., Stephanson, O., Ljundggren, C., 1992. Regional pattern of tectonic stress in Europe. J. Geophys. Res. 97 (B8), 11,783–11,803.

Müller, B., Wehrle, V., Zeyen, H., Fuchs, K., 1997. Short-scale variations of tectonic regimes in the western European stress province north of the Alps and Pyrenees. Tectonophysics 275, 199–219.

Nicolas, M., Santoire, J.P., Delpech, P.Y., 1990. Intraplate seismicity: new seismotectonic data in Western Europe. Tectonophysics 179, 27–53.

Nocquet, J.M., Calais, Altamimi, Z., Sillard, P., Boucher, C., 2001. Intraplate deformation in western Europe deduced from an analysis of the International Terrestrial Reference Frame 1997 (ITRF97) velocity field. J. Geophys. Res. 106 (B6), 11239–11257.

Nocquet, J.M., Calais, 2003. Crustal velocity field of western Europe from permanent GPS array solutions, 1996–2001. J. Geophys. Res. 154, 72–88.

Pavoni, N., 1980. Crustal stresses inferred from fault-plane solutions of earthquakes and neotectonic formation in Switzerland. Rock Mech. 9, 63–68.

Pfiffner, O.A., Lehner, P., Heitzmann, P., Müller, St., Steck, A., 1997. Deep Structure of the Alps, Results of NRP20, 380. Birkhaüser, Basel, Switzerland.

Plenefisch, T., Bonjer, K.P., 1997. The stress field in the Rhine graben area inferred from earthquake focal mechanisms and estimation of frictional parameters. Tectonophysics 275, 71–97.

Regenauer-Lieb, K., Petit, J.-P., 1997. Cutting of the European continental lithosphere: plasticity theory applied to the present Alpine collision. J. Geophys. Res. 102, 7731–7748.

Ritter, J.R.R., Jordan, M., Christiensen, U.R., Achauer, U., 2001. A mantle plume below the Eifel volcanic fields, Germany. Earth Planet. Sci. Lett. 186, 7–14.

Rózsa, Sz., Heck, B., Mayer, M., Seitz, K., Westrhaus, M., Zipelt, K., 2004. Determination of displacements in the Upper Rhine Graben area from GPS and levelling data. Int. J. Earth Sci. 94 (4), 538–549.

Schlatter, A., Schneider, D., Geiger, A., Kahle, H.-G., 2004. Recent vertical movements from precise levelling in the vicinity of the city of Basle, Switzerland. Int. J. Earth Sci. 94 (4), 507–514.

Schmid, S.M., Pfiffner, O.A., Froitzheim, N., Schoenborn, G., Kissling, E., 1996. Geophysical-geological transect and tectonic evolution of the Swiss-Italian Alps. Tectonics 15 (5), 1036–1064.

Schmid, S.M., Pfiffner, O.A., Schreurs, G., 1997. Rifting and collision in the Penninic zone of eastern Switzerland. In: Deep Structure of the Alps results of NRP20, Birkhäuser, Basel, Switzerland, pp. 160–185.

Schumacher, M.E., 2002. Upper Rhine Graben: role of preexisting structures during rift evolution. Tectonics 21 (1), 1–17.

Sobolev, S.V., Zeyen, H., Granet, M., Achauer, U., Bauer, Ch., Werling, F., Altherr, R., Fuchs, K., 1997. Upper mantle temperatures and lithosphere-asthenosphere system beneath the France Massif Central constrained by seismic, gravity, petrologic and thermal observations. Tectonophysics 275, 143–164.

Straub, Ch.S., 1996. Recent Crustal Deformation and Strain in the Marmara Sea Region, NW Anatolia Inferred from GPS Measurements. Ph.D. Dissertation. ETH Zürich.

Sue, C., Thouvenot, F., Fréchet, J., Tricart, P., 1999. Widespread extension in the core of the western Alps revealed by earthquake analysis. J. Geophys. Res. 104 (B11), 25,611–25,622.

Sue, C., Tricart, P., 2003. Neogene to ongoing normal faulting in the inner western Alps: a major evolution of the late alpine tectonics. Tectonics 22 (5), 1–25.

Tesauro, M., Hollenstein, Ch., Egli, R., Geiger, A., Kahle, H.-G., 2005. Continuous GPS and broad-scale deformation across the Rhine Graben and the Alps. Int. J. Earth Sci. 94 (4), 525–537.

Vigny, C., Chéry, J., Duquesnoy, T., Jouanne, F., Amman, J., Anzdei, M., Avouac, J.-P., Barlier, F., Bayer, R., Briole, P., Calais, E., Cotton, F., Duquenne, F., Feigl, K.L., Ferhat, G., Flouzat, M., Gamond, J.-F., Geiger, A., Harmel, A., Kasser, M., Laplanche, M., Le Pape, M., Martinod, J., Ménard, G., Meyer, B., Ruegg, J.-C., Scheubel, J.-M., Scotti, O., Vidal, G., 2002. GPS network monitors the western Alps deformation over a five-year period: 1993–1998. J. Geodesy 76, 63–76.

Villemin, T., Alvarez, F., Angelier, J., 1986. The Rhinegraben: extension, subsidence and shoulder uplift. Tectonophysics 128, 47–59.

Villemin, T., Coletta, B., 1990. Subsidence in the Rhine Graben: a new compilation of borehole data. In: Symposium on Rhine-Rhone Rift system; ICL-WG3 Symp. (23–24 March 1990), Abstracts. Geol. Inst. Univ. Basel, 31.

Wiens, D.A., Stein, S., 1985. Implications of oceanic intraplate seismicity for plate stresses, driving forces and rheology. Tectonophysics 116, 143–162.

Zeyen, H., Volker, F., Wehrle, V., Fuchs, K., Sobolev, S.V., 1997. Styles of continental rifting: crust–mantle detachment and mantle plumes. Tectonophysics 278, 329–352.

Ziegler, P.A., 1992. European cenozoic rift system. Tectonophysics 208, 91–111.

Ziegler, P.A., Dèzes, P., 2004. The Rhine rift system: evolution of the lithosphere. Int. J. Earth Sci. 94 (4), 594–614.

Zippelt, K., Mälzer, H., 1981. Recent height changes in the central segment of the Rhinegraben and its adjacent shoulders. Tectonophysics 73, 119–123.